Supplementary Materials

The Atmospheric Oxidizing Capacity in China:
Part 2. Sensitivity to emissions of primary pollutants

Jianing Dai[a], Guy P. Brasseur[a,e,f], Mihalis Vrekoussis[b,g,h], Maria Kanakidou [b,d], Kun Qu[b], Yijuan Zhang[b], Hongliang Zhang[c], Tao Wang[f]

[a] Environmental Modelling Group, Max Planck Institute for Meteorology, Hamburg, 20146, Germany

[b] Institute of Environmental Physics (IUP), University of Bremen, Bremen, 28359, Germany

[c] Department of Environmental Science and Engineering, Fudan University, 200433, China

[d] Environmental Chemical Processes Laboratory, Department of Chemistry, University of Crete, Heraklion, 70013, Greece

[e] National Center for Atmospheric Research, Boulder, Colorado, 80307, USA

[f] Department of Civil and Environmental Engineering, The Hong Kong Polytechnic University, Hong Kong, China

[g] Center of Marine Environmental Sciences (MARUM), University of Bremen, Germany

[h] Climate and Atmosphere Research Center (CARE-C), The Cyprus Institute, Nicosia, Cyprus

Correspondence to: Guy P. Brasseur (guy.brasseur@mpimet.mpg.de)

Table S1. Chemical species in the emission input of MOZART_MOSAIC scheme

	Chemical species in emission input
NO$_x$	E_NO, E_NO2
AVOCs	E_C2H4, E_C3H6, E_BIGENE, E_C2H6, E_C3H8, E_BIGALK, E_BENZENE, E_TOLUENE, E_XYLENE, E_C2H2, E_MACR, E_CH3CHO, E_C2H5OH, E_CH3OH, E_C10H16, E_CH3COCH3, E_MVK
Other	E_CO, E_NH3, E_SO2
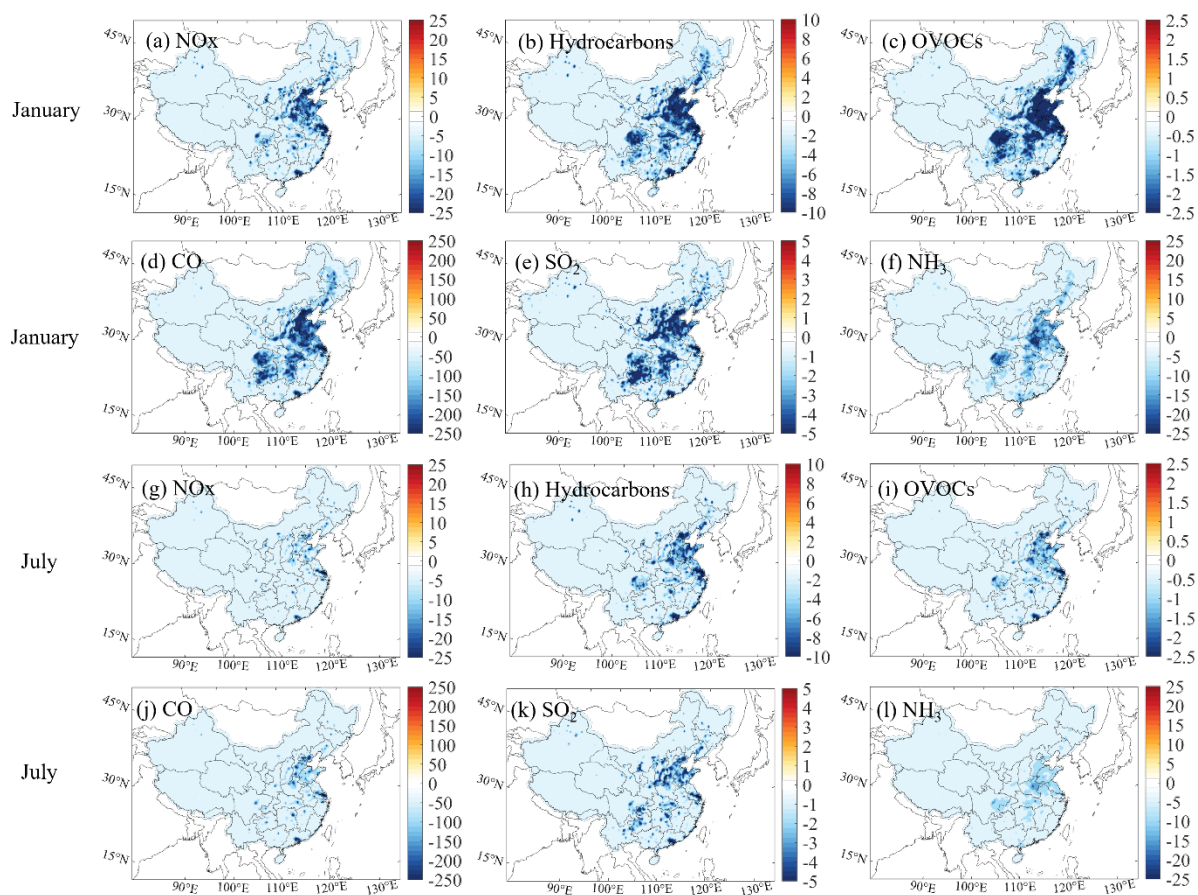
Figure S1. Changes in the model input of anthropogenic nitrogen oxides (NO_x; a, g), Hydrocarbons (b, h), oxidized volatile organic components (OVOCs; c, i), carbon monoxide (CO; d, j), sulfur dioxide (SO_2; e, k), and ammonia (NH_3; f, l) in January and July of 2018. Units are in mole km_2^{-1} hr^{-1}.
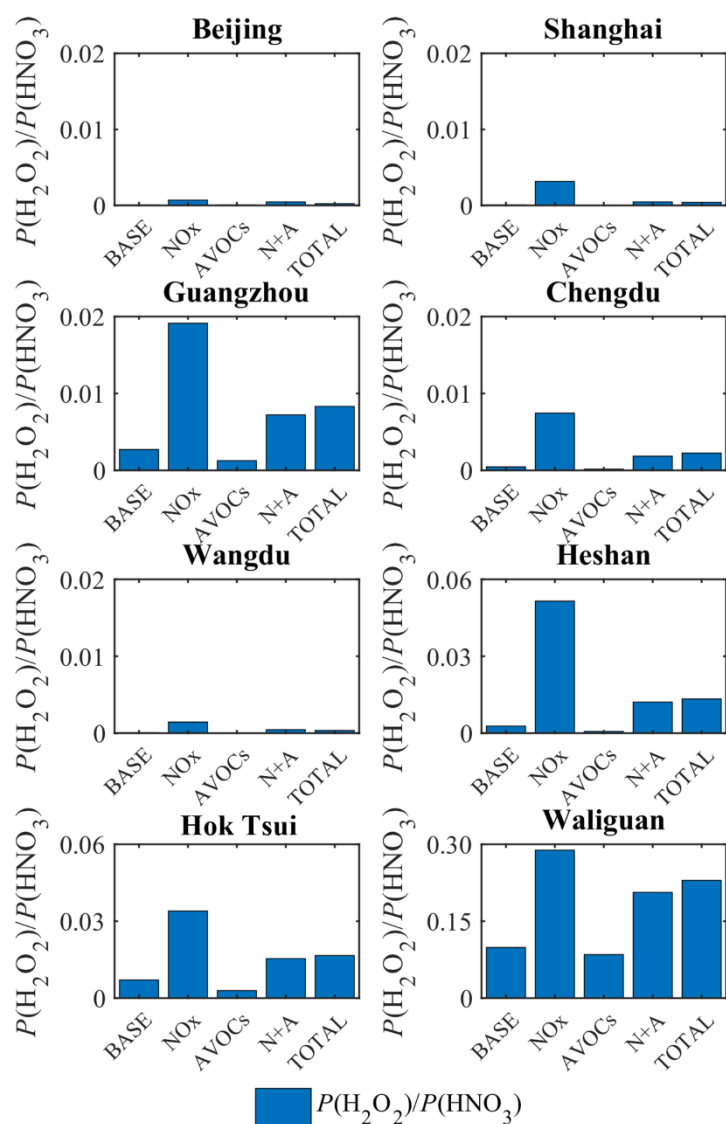
Figure S2. The daytime (06:00 to 19:00 Local Standard Time (LST)) value of ratio between the production rate of hydrogen peroxide (H_2O_2) and nitric acid (HNO_3) [$P(H_2O_2)/P(HNO_3)$] in five different simulated cases (BASE, NOx, AVOCs, N+A, TOTAL cases) and in eight different sites (urban, rural and remote sites) in January of 2018.
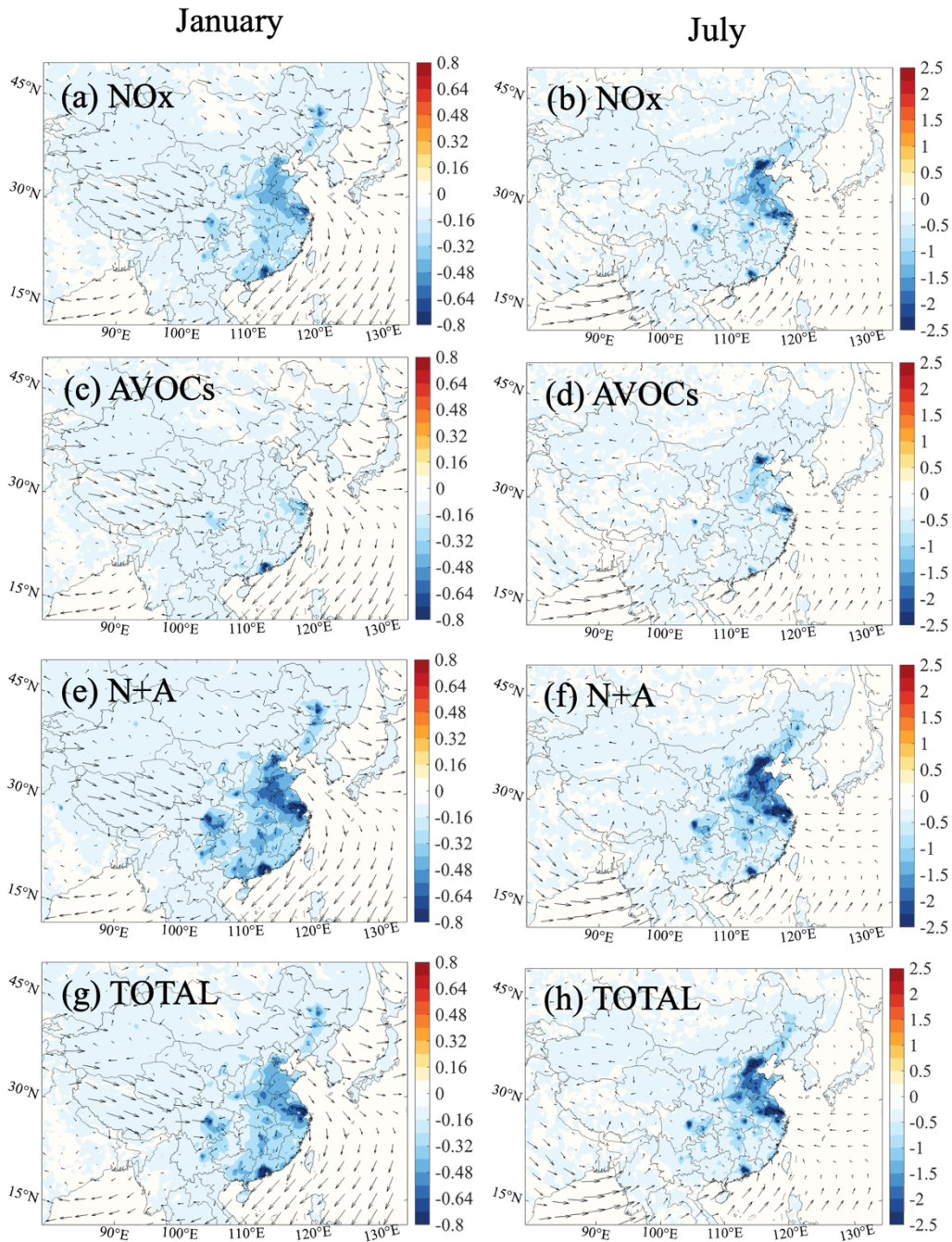
Figure S3. Changes in the surface destruction rate of RO_x ($D(RO_x)$; RO_2+HO_2+OH) [Unit: ppbv h^{-1}] response to the ratio of 0.5 in NO_x emissions (a, b; NO_x case), in Anthropogenic VOCs (AVOCs) emissions (c, d; AVOCs case), in NO_x and AVOCs emissions (e, f; N+A case), and in all anthropogenic emissions (g, h, TOTAL case) relative to BASE case. The results are shown for January (a, c, e, g) and July (b, d, f, h) of 2018. Arrows represent the wind speed and wind direction scaled by a factor of 5.
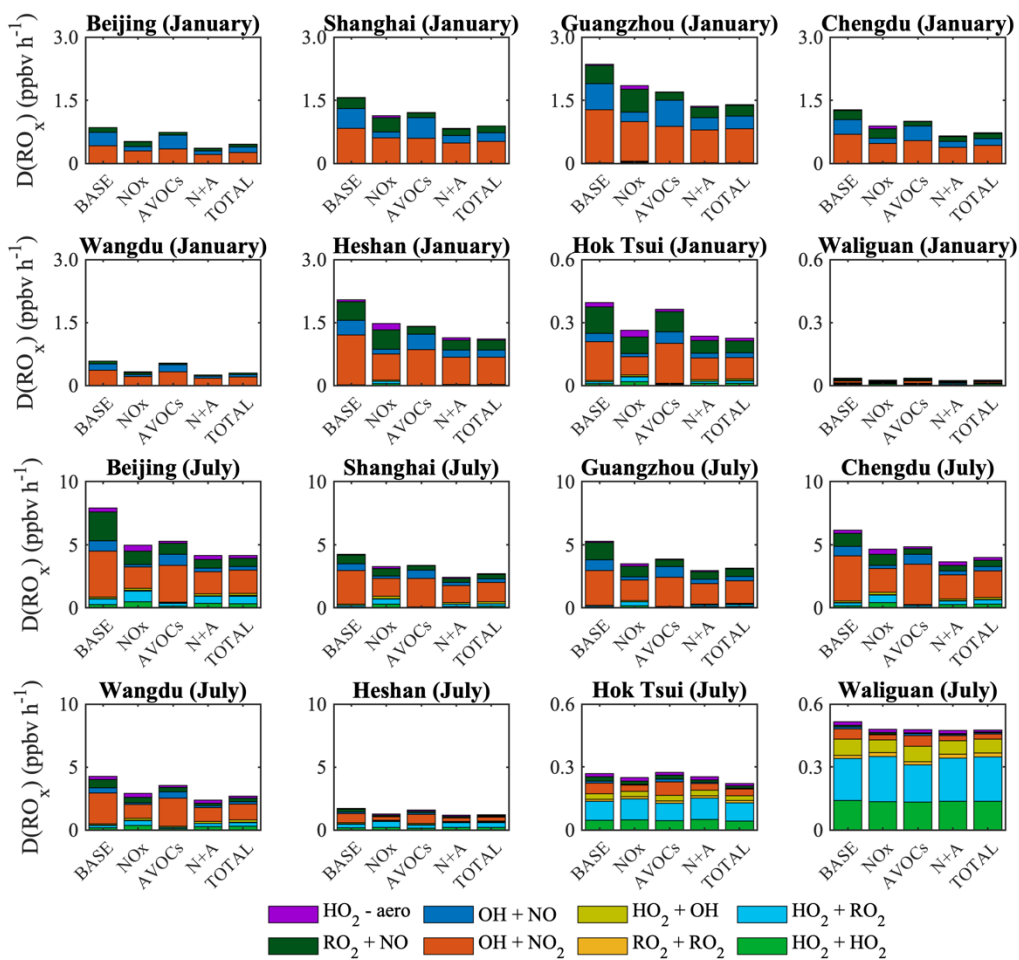
Figure S4. Averaged daytime value of the destruction rate of RO_x ($D(RO_x)$) [Unit: ppbv h^{-1}] in five different simulated cases (BASE, NOx, AVOCs, N+A, TOTAL cases) and in eight different sites (urban, rural and remote sites) in January and July of 2018.
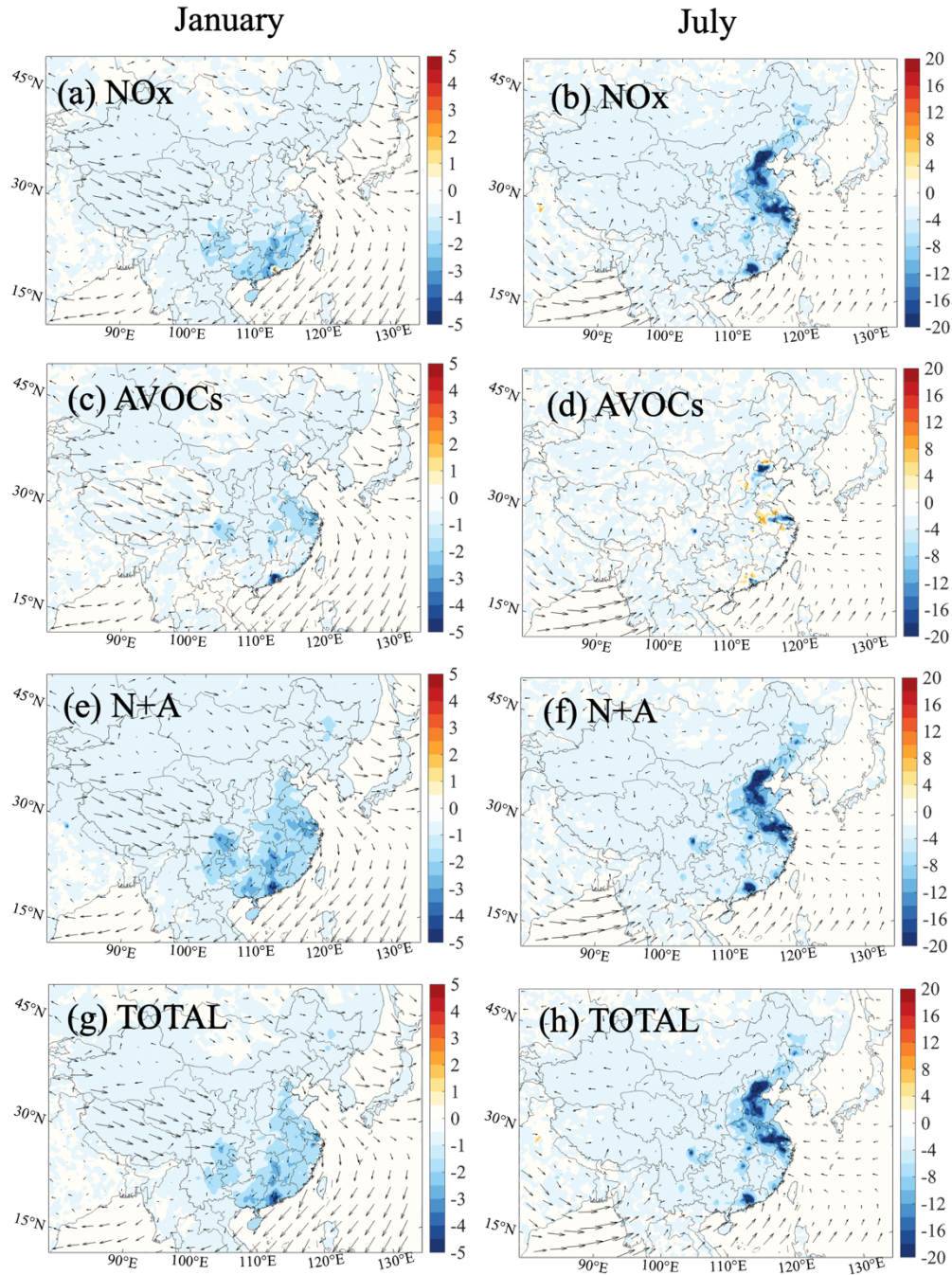
Figure S5. Changes in the surface production rate of odd oxygen ($P(O_x)$) [Unit: ppbv h^{-1}] response to the ratio of 0.5 in NO$_x$ emissions (a, b; NO$_x$ case), in Anthropogenic VOCs (AVOCs) emissions (c, d; AVOCs case), in NO$_x$ and AVOCs emissions (e, f; N+A case), and in all anthropogenic emissions (g, h, TOTAL case) relative to BASE case. The results are shown for January (a, c, e, g) and July (b, d, f, h) of 2018. Arrows represent the wind speed and wind direction scaled by a factor of 5.
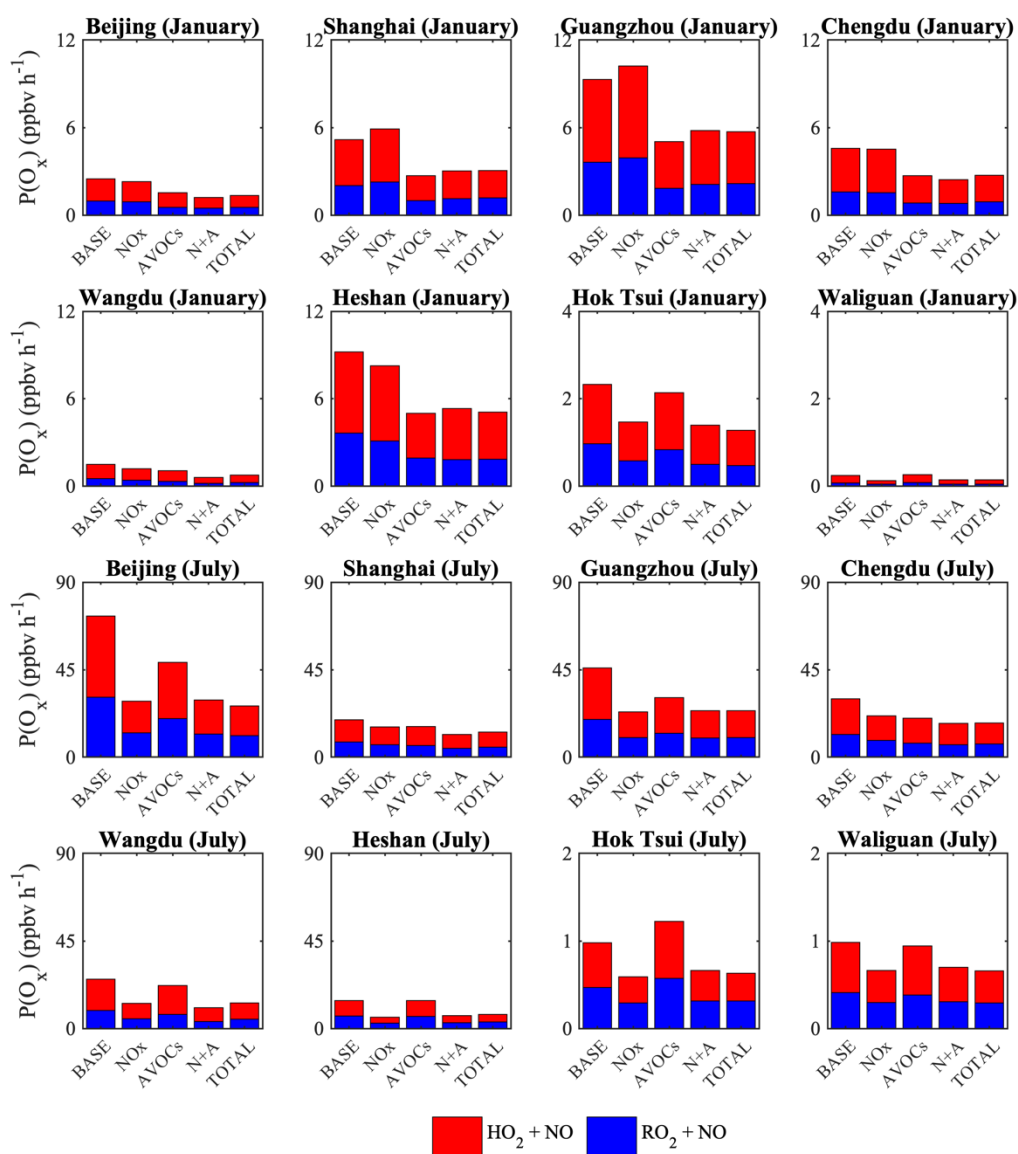
Figure S6. Averaged daytime value of the production rate of odd oxygen ($P(O_x)$ [Unit: ppbv h^{-1}] in five different simulated cases (BASE, NOx, AVOCs, N+A, TOTAL cases) and in eight different sites (urban, rural and remote sites) in January and July of 2018.
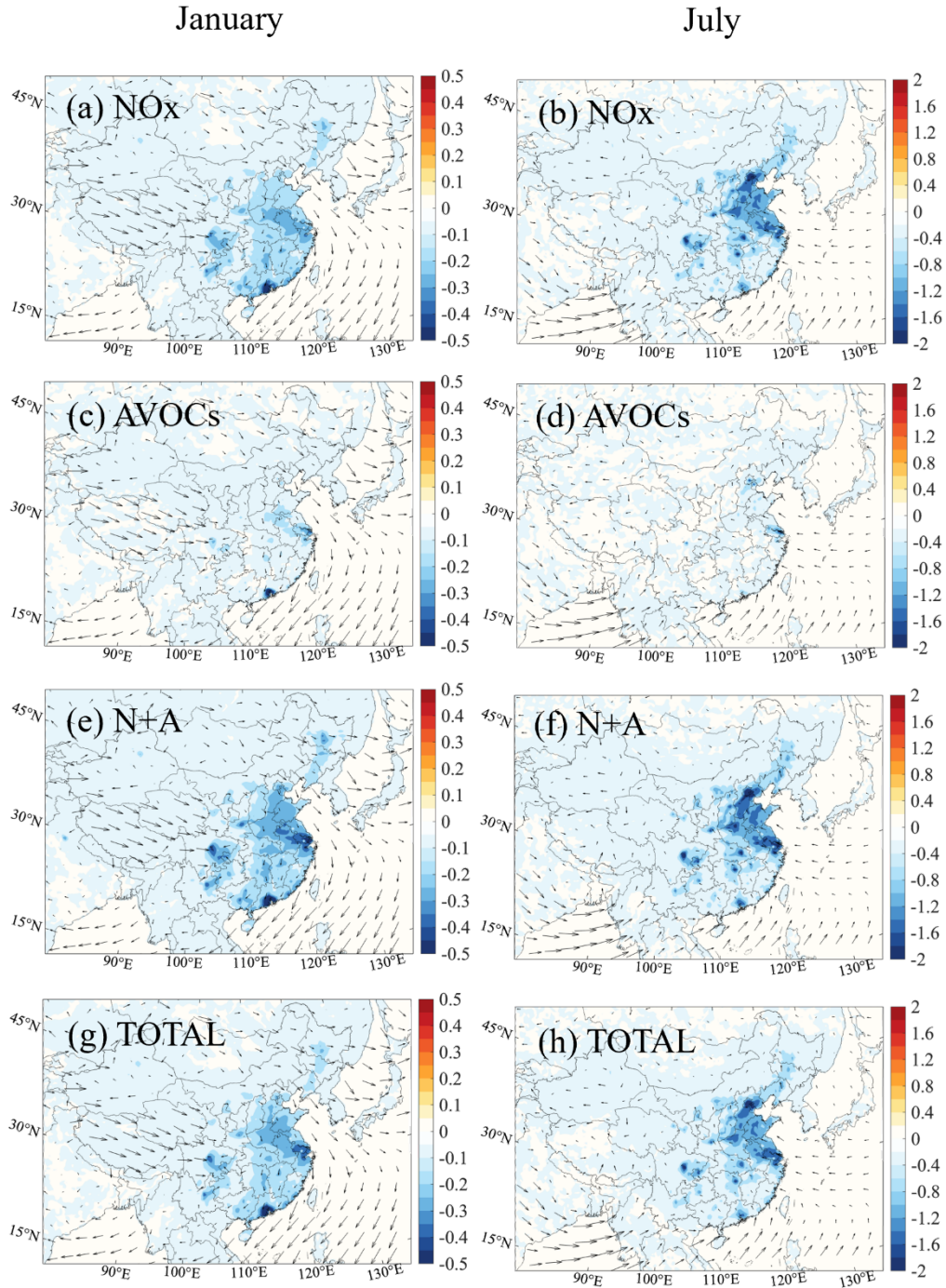
Figure S7. Changes in the surface destruction rate of O_x ($D(O_x)$) [Unit: ppbv h^{-1}] response to the ratio of 0.5 in NO$_x$ emissions (a, b; NO$_x$ case), in Anthropogenic VOCs (AVOCs) emissions (c, d; AVOCs case), in NO$_x$ and AVOCs emissions (e, f; N+A case), and in all anthropogenic emissions (g, h, TOTAL case) relative to BASE case. The results are shown for January (a, c, e, g) and July (b, d, f, h) of 2018. Arrows represent the wind speed and wind direction scaled by a factor of 5.

January   July
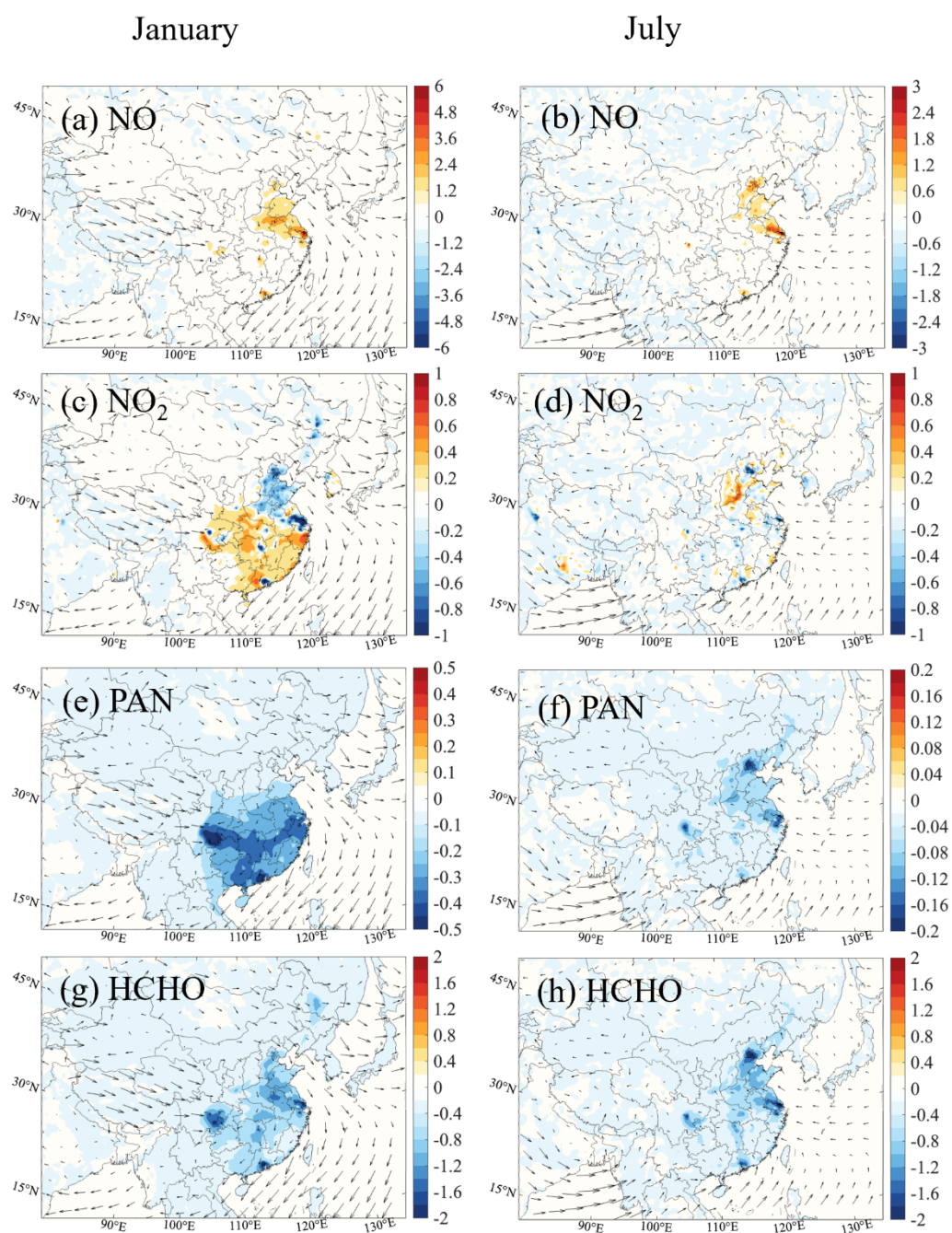
Figure S8. Changes in the surface mixing ratio of NO (a, b) [unit: ppbv] and NO$_2$ (c, d) [Unit: ppbv], peroxyacyl nitrate (PAN; a, b) [Unit: ppbv] and formaldehyde (HCHO; c, d) [Unit: ppbv] response to the AVOCs case relative to BASE case. The results are shown for January (a, c, e, g) and July (b, d, f, h) of 2018. Arrows represent the wind speed and wind direction.
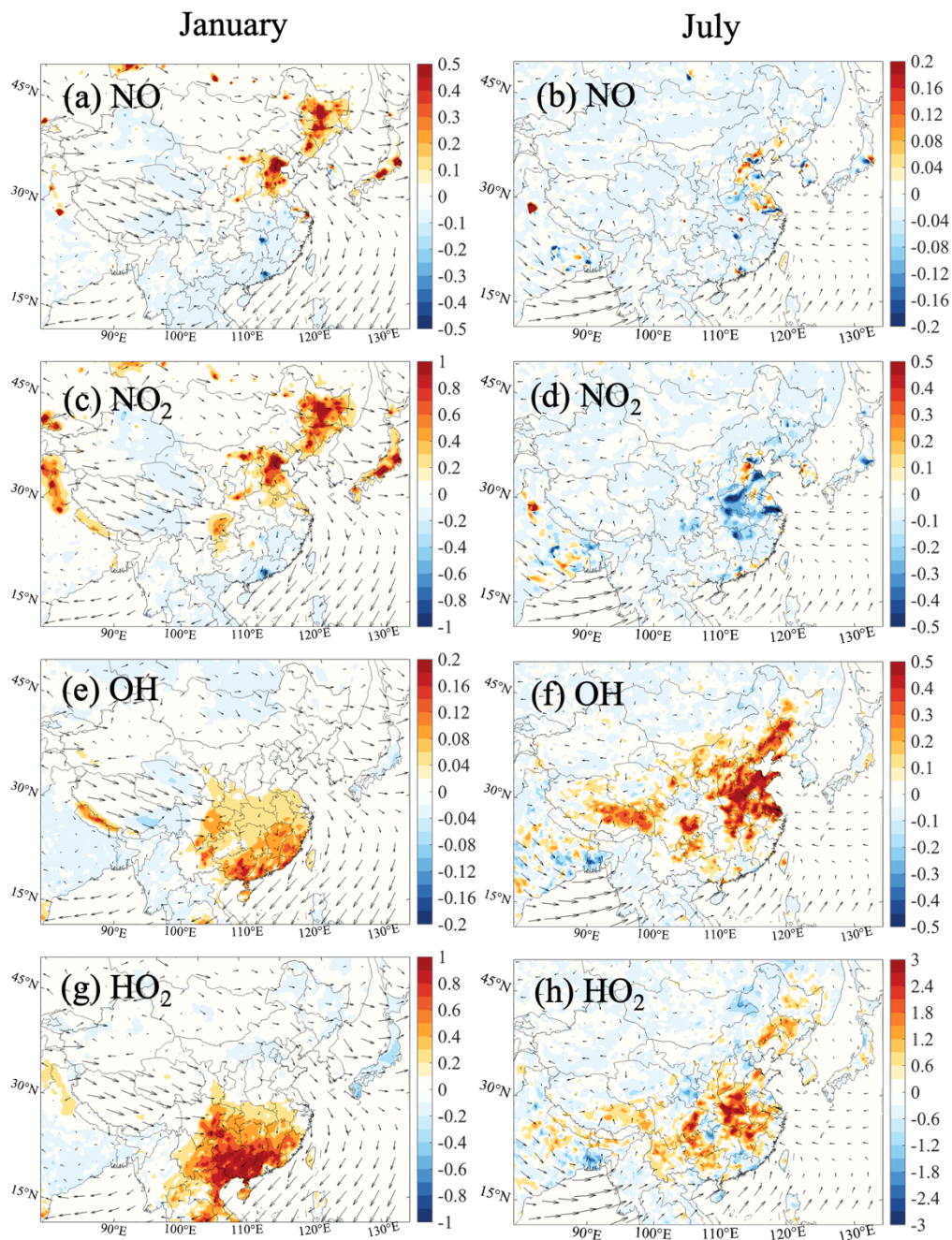
Figure S9. Changes in the surface mixing ratio of NO (a, b) [Unit: ppbv], NO$_2$ (c, d) [Unit: ppbv], OH radical (e, f) [Unit: 0.1 pptv] and HO$_2$ radical (g, h) [Unit: pptv] response to the TOTAL case relative to N+A case. Results are shown for January (a, c, e, g) and July (b, d, f, h) of 2018. Arrows represent the wind speed and wind direction.
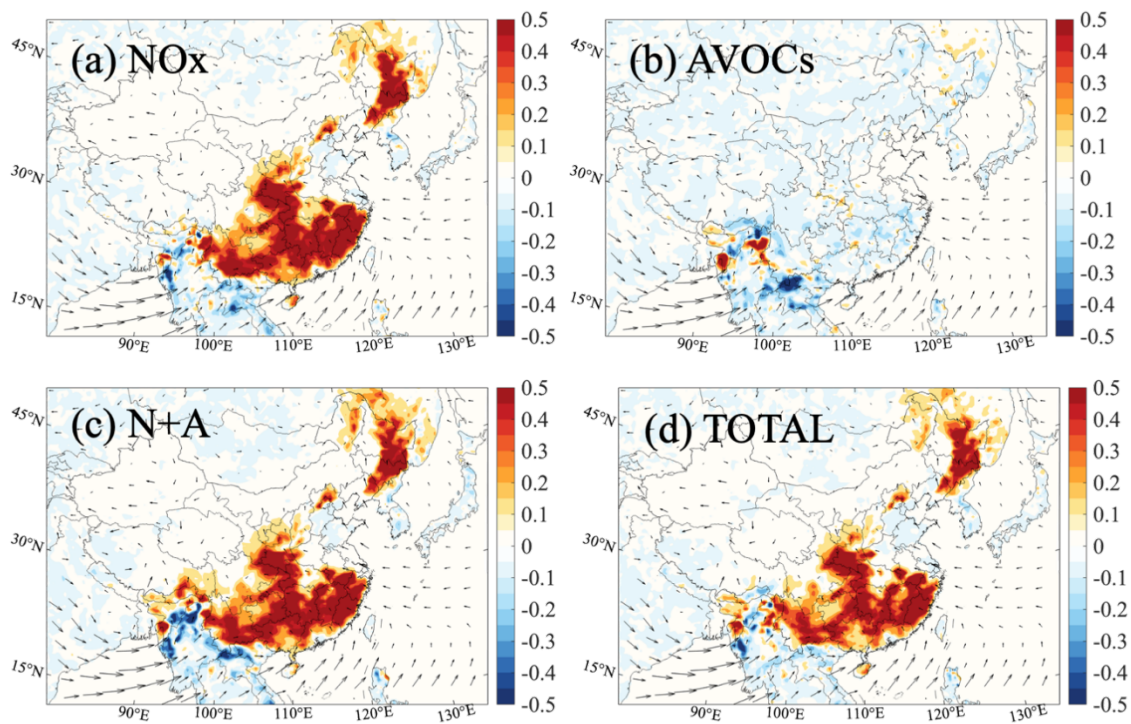
Figure S10. Changes in the averaged surface mixing ratio of isoprene [Unit: ppbv] response to in NO_x case (a) relative to BASE case in the July of 2018. Arrows represent the wind speed and wind direction.
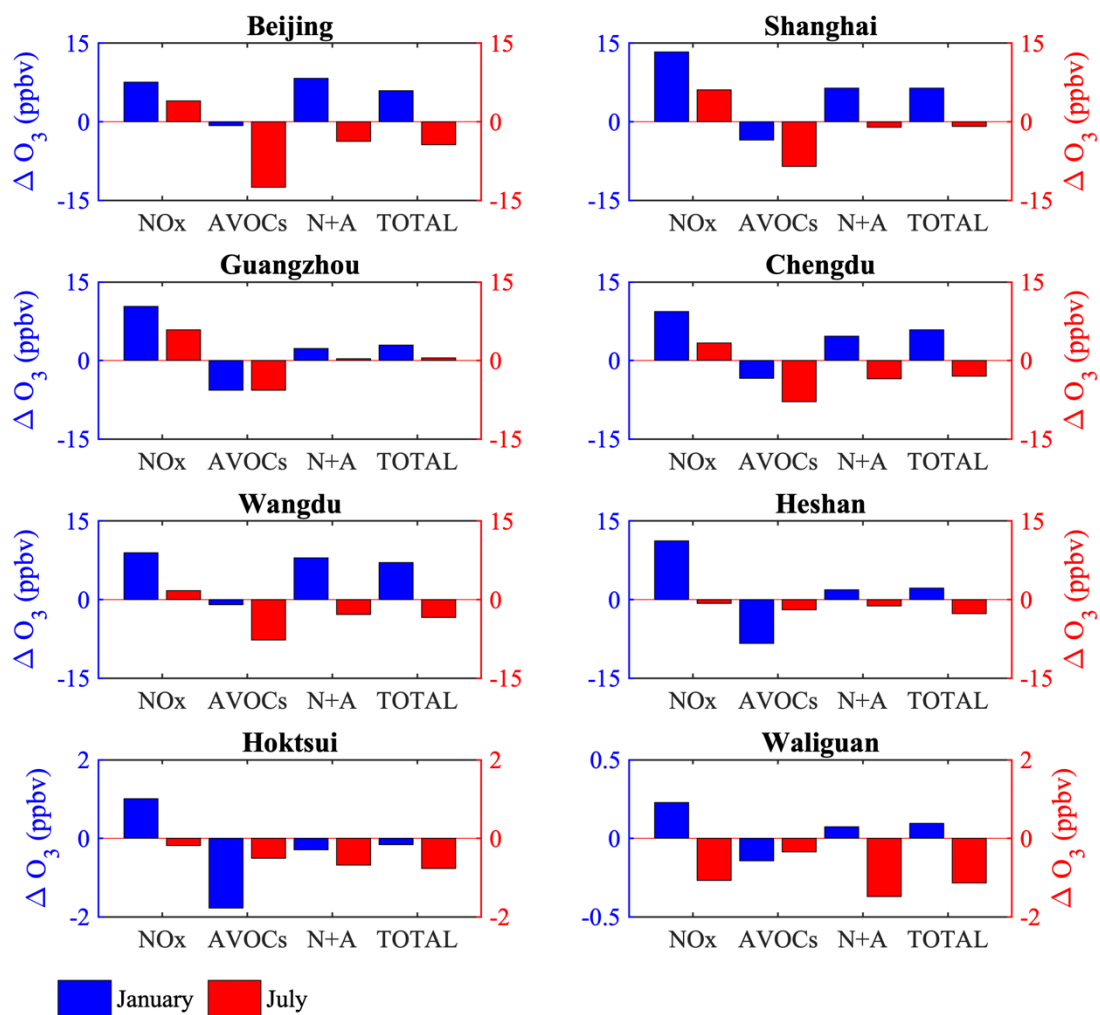
Figure S11. Changes in the averaged surface mixing ratio of ozone during daytime in five different simulated cases (BASE, NOx, AVOCs, N+A, TOTAL cases) and in eight different sites in January and July of 2018.
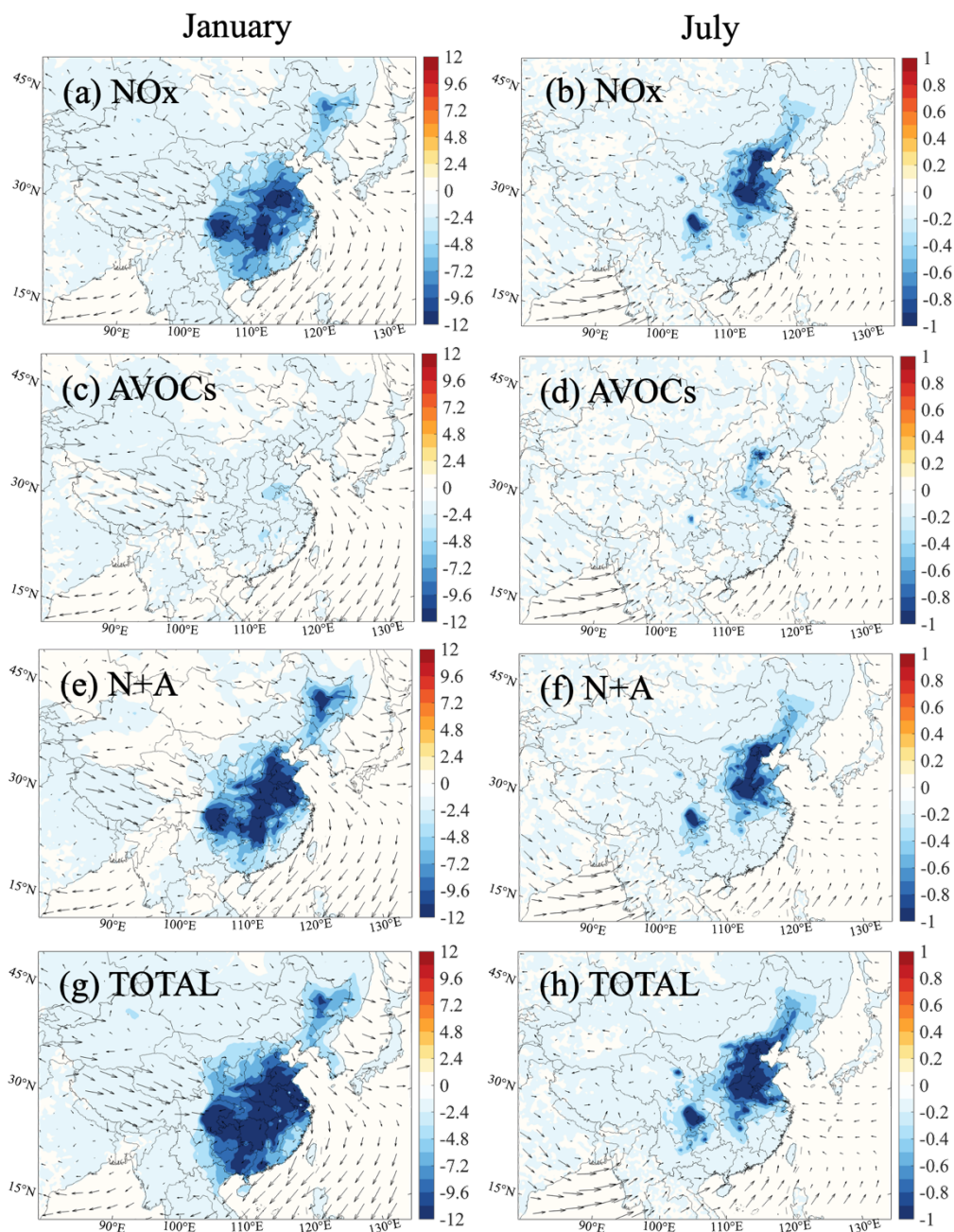
Figure S12. Spatial distribution of particulate nitrate [NO₃⁻; Unit: μg m⁻³] response to the ratio of 0.5 in NOₓ emissions (a, b; NOₓ case), in Anthropogenic VOCs (AVOCs) emissions (c, d; AVOCs case), in NOₓ and AVOCs emissions (e, f; N+A case), and in all anthropogenic emissions (g, h, TOTAL case) relative to BASE case. The results are shown for January (a, c, e, g) and July (b, d, f, h) of 2018. Arrows represent the wind speed and wind direction scaled by a factor of 5.
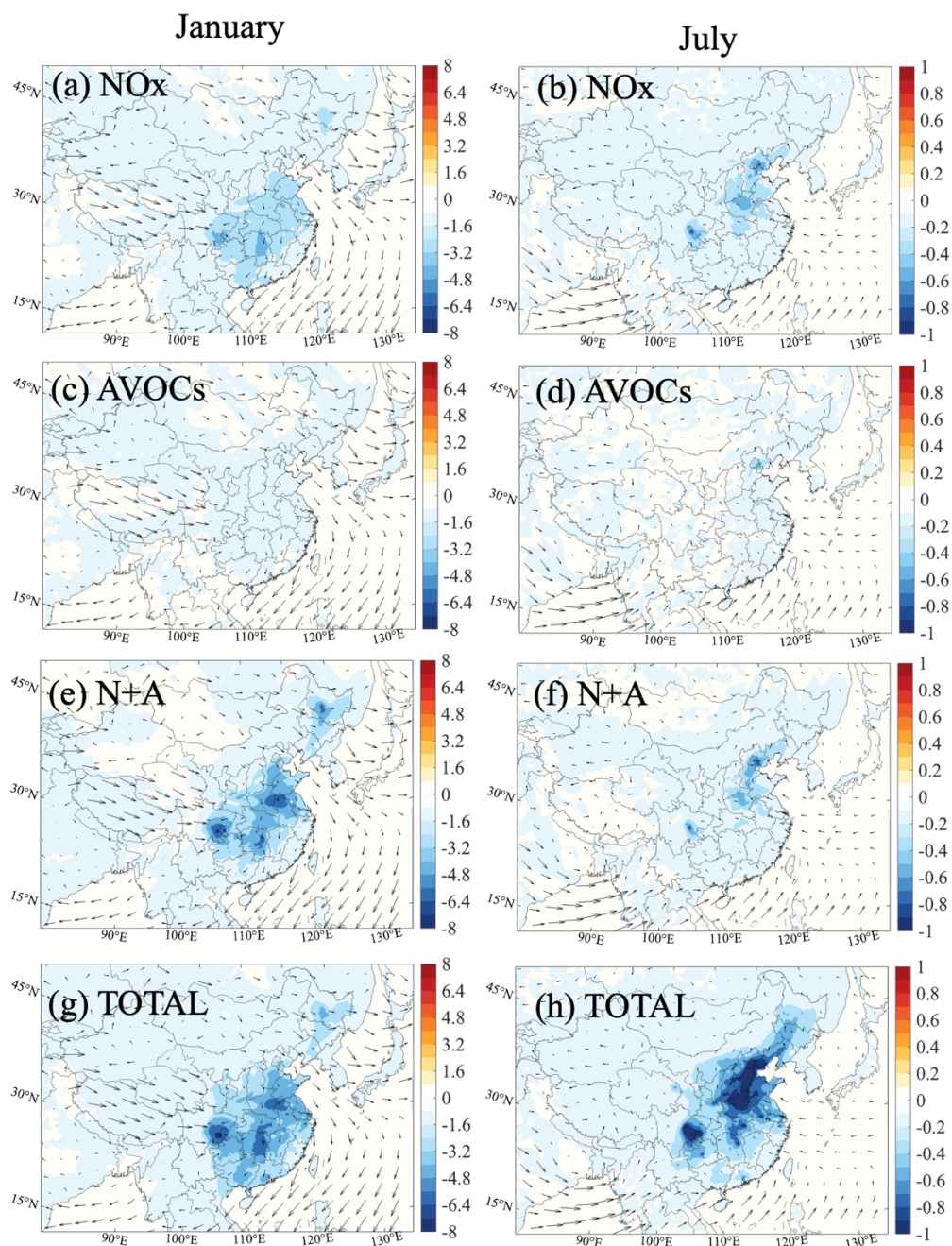
Figure S13. Spatial distribution of particulate ammonia [NH$_4^+$; Unit: μg m^{-3}] response to the ratio of 0.5 in NO$_x$ emissions (a, b; NO$_x$ case), in Anthropogenic VOCs (AVOCs) emissions (c, d; AVOCs case), in NO$_x$ and AVOCs emissions (e, f; N+A case), and in all anthropogenic emissions (g, h, TOTAL case) relative to BASE case. The results are shown for January (a, c, e, g) and July (b, d, f, h) of 2018. Arrows represent the wind speed and wind direction scaled by a factor of 5.
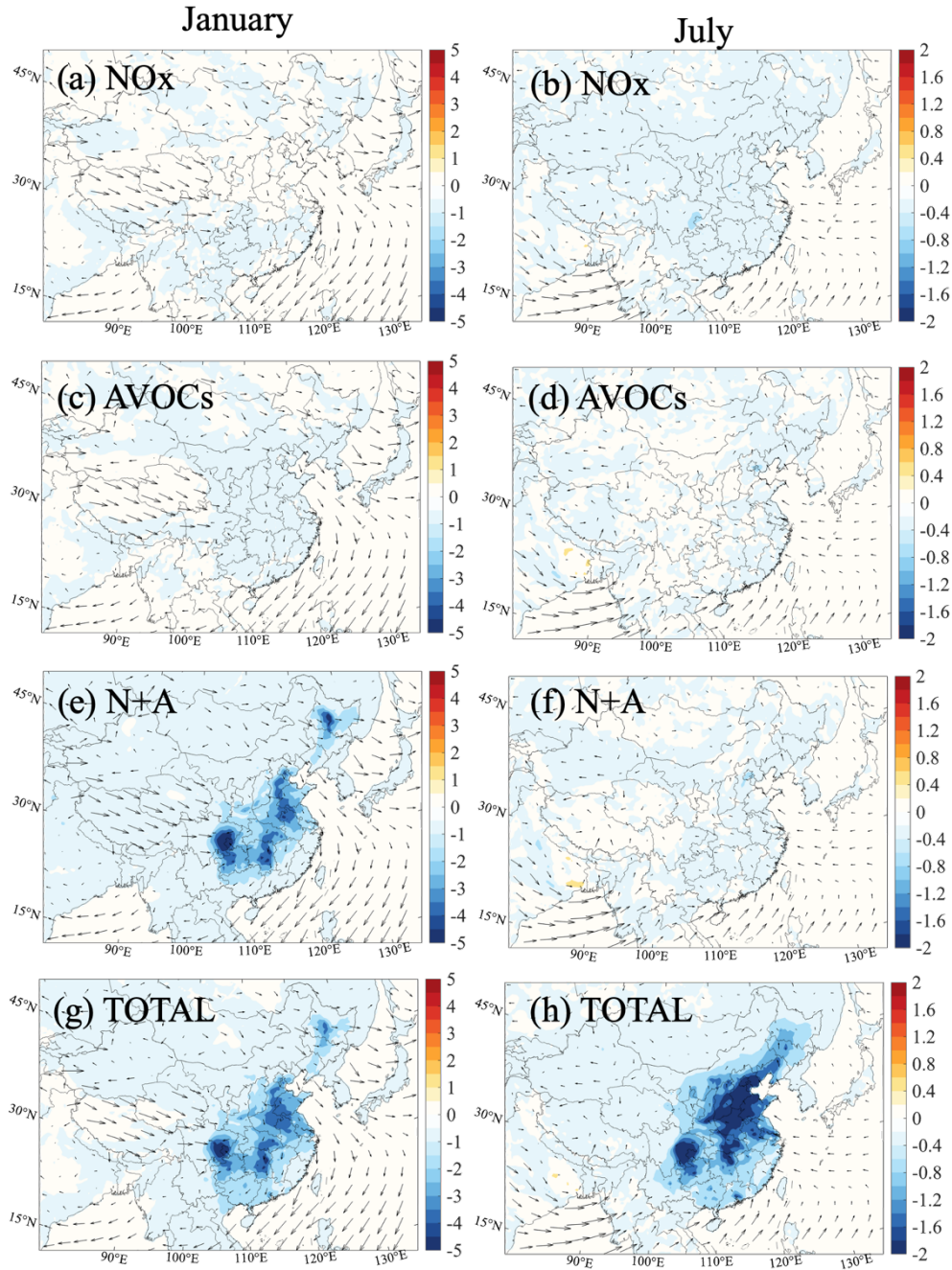
Figure S14. Spatial distribution of particulate sulfate [SO_4^{2-}; Unit: μg m^{-3}] response to the ratio of 0.5 in NO$_x$ emissions (a, b; NO$_x$ case), in Anthropogenic VOCs (AVOCs) emissions (c, d; AVOCs case), in NO$_x$ and AVOCs emissions (e, f; N+A case), and in all anthropogenic emissions (g, h, TOTAL case) relative to BASE case. The results are shown for January (a, c, e, g) and July (b, d, f, h) of 2018. Arrows represent the wind speed and wind direction scaled by a factor of 5.
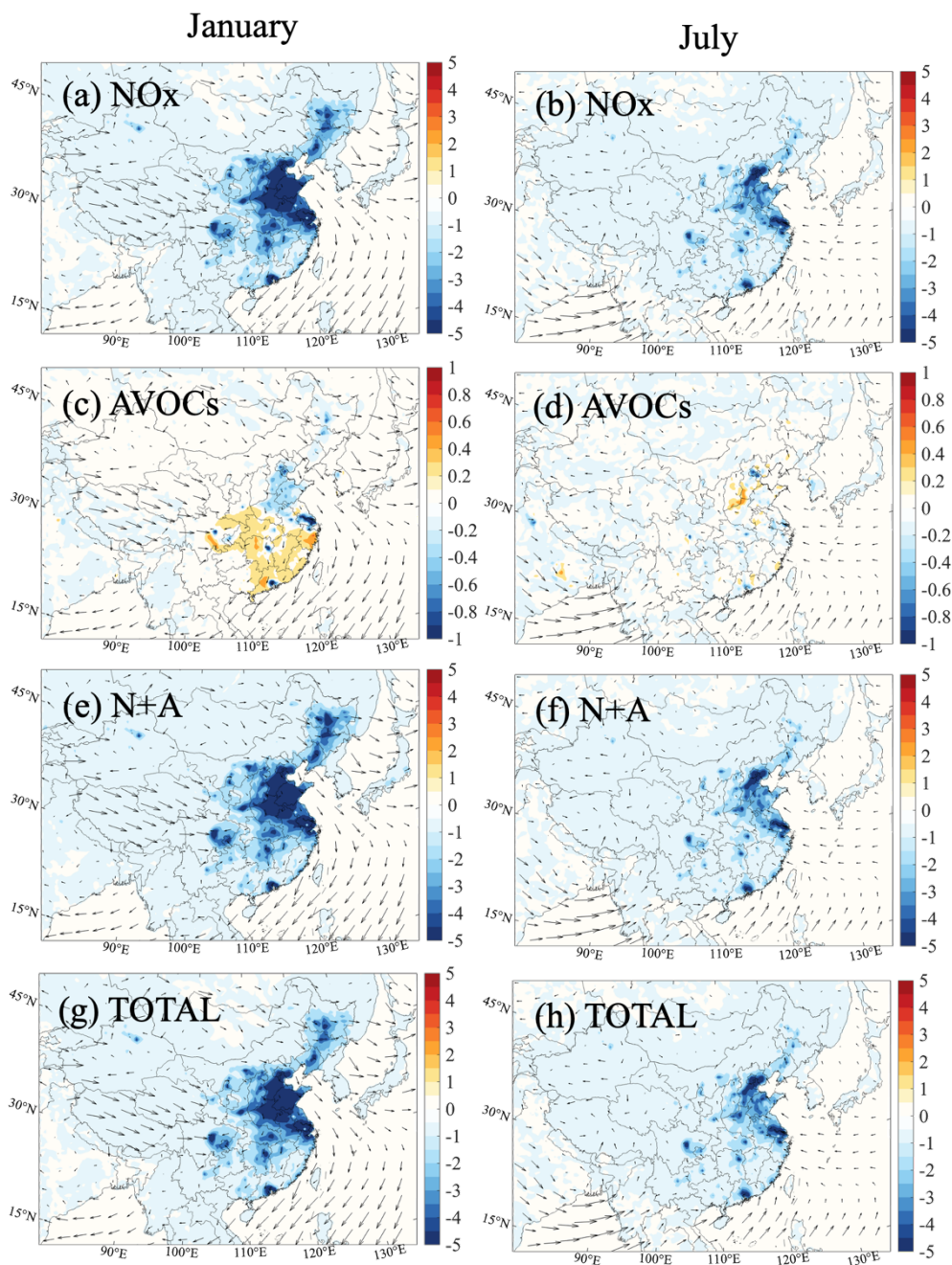
Figure S15. Changes in the averaged daytime OH reactivity from NO_x [Unit: s^{-1}] response to the NO_x case (a, b), AVOCs case (c, d), N+A case (e, f), and TOTAL case (g, h) relative to BASE case. The results are shown for January (a, c, e, g) and July (b, d, f, h) of 2018. Notice the inconsistency in scale of Figure S17 c and d. Arrows represent the wind speed and wind direction scaled by a factor of 5.
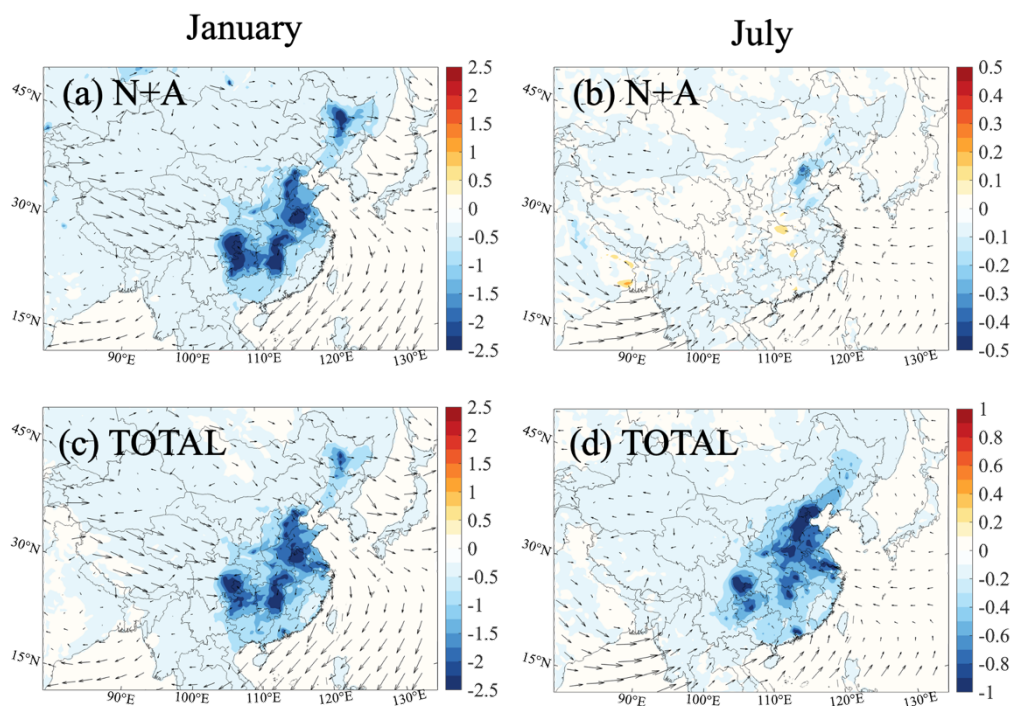
Figure S16. Changes in the averaged daytime OH reactivity from CO [Unit: s^{-1}] response to N+A case (e, f) and TOTAL case (g, h) relative to the BASE case. The results are shown for January (a, c) and July (b, d) of 2018. Notice the inconsistency in the scale. Arrows represent the wind speed and wind direction.
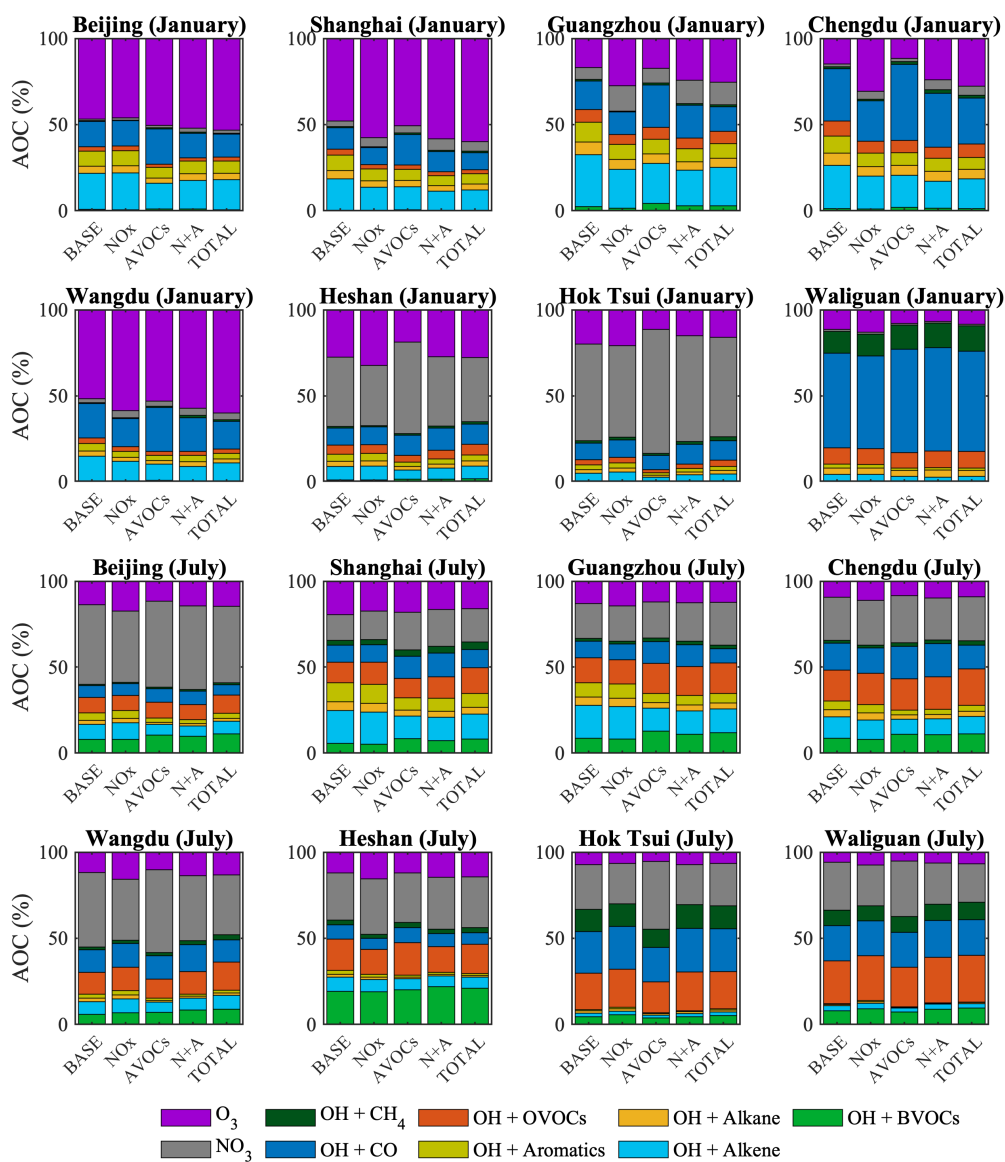
Figure S17. Relative terms of nighttime *AOC* [Unit: %] contributed from nine types of reactions in five different simulated cases (BASE, NOx, AVOCs, N+A, TOTAL cases) and in eight different sites in January and July of 2018.
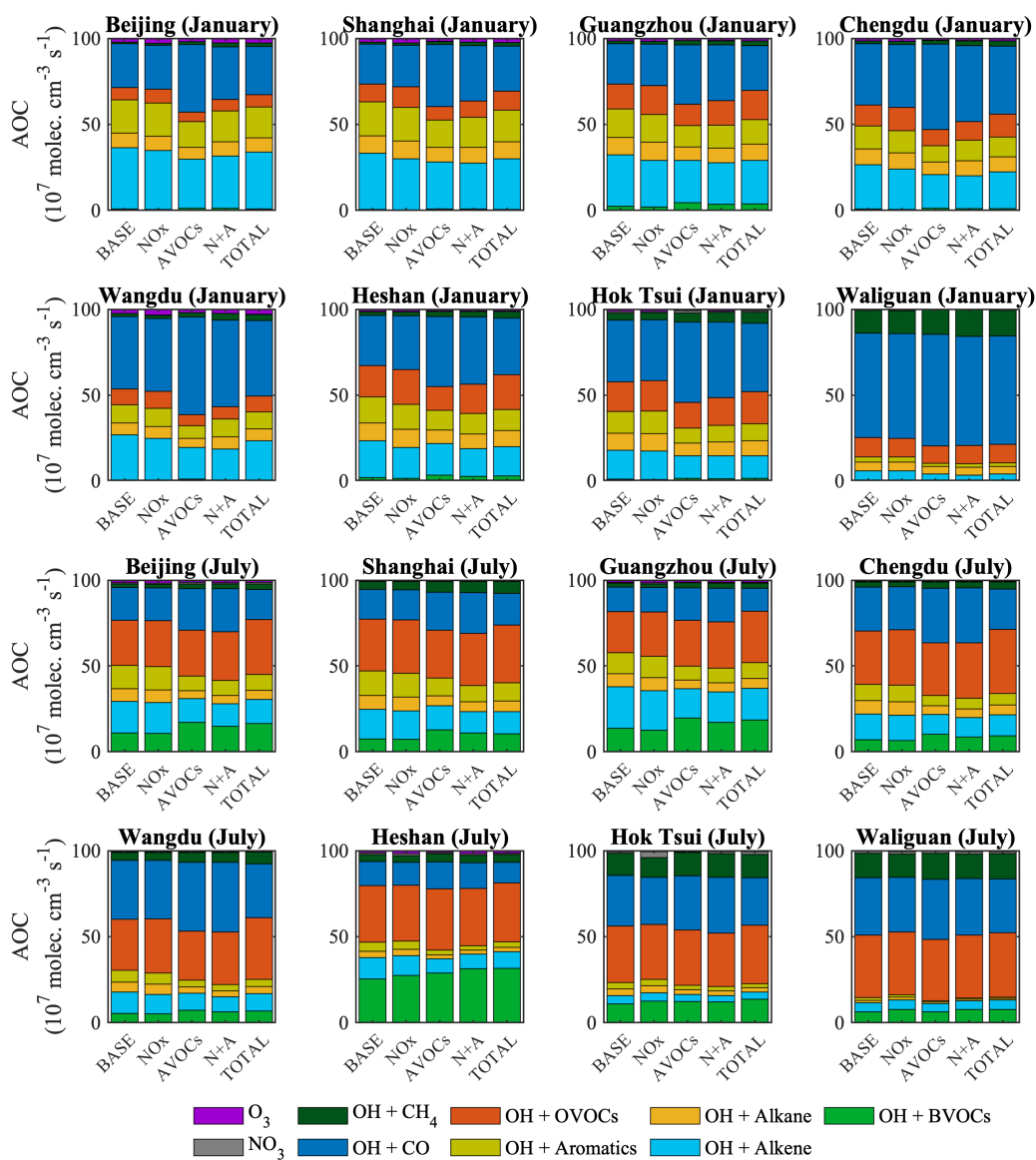
Figure S18. Relative terms of averaged daytime *AOC* [Unit: %] contributed from nine types of reactions in five different simulated cases (BASE, NOx, AVOCs, N+A, TOTAL cases) and in eight different sites in January and July of 2018.